Quantum Jumps in the Non-Hermitian Dynamics of a Superconducting Qubit

Weijian Chen,[1,2,*] Maryam Abbasi,[1] Yogesh N. Joglekar ®,[3] and Kater W. Murch ®[1,2,†]

[1]*Department of Physics, Washington University, St. Louis, Missouri 63130, USA*
[2]*Center for Quantum Sensors, Washington University, St. Louis, Missouri 63130, USA*
[3]*Department of Physics, Indiana University-Purdue University Indianapolis, Indianapolis, Indiana 46202, USA*

We study the dynamics of a driven non-Hermitian superconducting qubit which is perturbed by quantum jumps between energy levels, a purely quantum effect with no classical correspondence. The quantum jumps mix the qubit states leading to decoherence. We observe that this decoherence rate is enhanced near the exceptional point, owing to the cube-root topology of the non-Hermitian eigenenergies. Together with the effect of non-Hermitian gain or loss, quantum jumps can also lead to a breakdown of adiabatic evolution under the slow-driving limit. Our study shows the critical role of quantum jumps in generalizing the applications of classical non-Hermitian systems to open quantum systems for sensing and control.

Dissipation is ubiquitous in nature; as in radioactive decay of an atomic nucleus and wave propagation in absorptive media, dissipation results from the coupling of these systems to different environmental degrees of freedom. These dissipative systems can be phenomenologically described by effective non-Hermitian Hamiltonians, where the non-Hermitian terms are introduced to account for the dissipation. The non-Hermiticity leads to a complex energy spectrum with the imaginary part quantifying the loss of particle or energy from the system. The degeneracies of a non-Hermitian Hamiltonian are known as exceptional points (EPs), where both the eigenvalues and the associated eigenstates coalesce [1,2]. The existence of EPs has been demonstrated in many classical systems [3–11] with applications in laser mode management [12–14], enhanced sensing [15–20], and topological mode transfer [21–24].

Though the effective Hamiltonian approach was developed decades ago as part of quantum measurement theory, recent experiments with single electronic spins [25,26], superconducting qubits [27], and photons [28–30] have expanded interest in uniquely quantum effects in non-Hermitian dynamics. Two approaches have been taken to study non-Hermitian dynamics in the quantum regime. The first is to simulate these dynamics—through a process known as Hamiltonian dilation—by embedding a non-Hermitian Hamiltonian into a larger Hermitian system [25,26,30]. A second approach is to directly isolate the non-Hermitian dynamics from a dissipative quantum system [27]. To understand this approach, recall that dissipative quantum systems are usually described by a Lindblad master equation that contains two dissipative terms: the first is a term that describes quantum jumps between the energy eigenstates of the system, and the second is a term that yields coherent nonunitary evolution [31–33]. By suppressing the former term, the resulting evolution is

described by an effective non-Hermitian Hamiltonian. This can be achieved through postselection to eliminate trajectories that contain quantum jumps [Fig. 1(a)] [27]. However, additional sources of energy dissipation or pure dephasing can alter this non-Hermitian evolution [34,35]. The combination of nonunitary dynamics and decoherence will lead to evolution that is starkly different than what is encountered with conventional open quantum systems. In this Letter, we characterize these dynamics using experiments on a superconducting qutrit. We observe quantum dynamics that result from the competition of the nonunitary effect of complex energies and quantum jumps. This leads to decoherence enhancement near the EP, nonstationary evolution of system eigenstates, and a quantum jump-induced breakdown of adiabaticity when a system parameter is slowly varied.
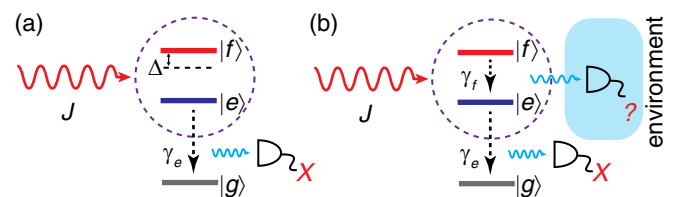

FIG. 1. (a) Formation of a non-Hermitian qubit through a dissipative three-level system. The ground level $|g\rangle$ acts as a continuum and can be used to monitor the quantum jumps from the $\{|e\rangle, |f\rangle\}$ submanifold. When postselection is used to eliminate this dynamics, the evolution in the $\{|e\rangle, |f\rangle\}$ submanifold is governed by a non-Hermitian Hamiltonian. J denotes the coupling rate from an applied drive with frequency detuning Δ relative to the $|e\rangle$–$|f\rangle$ transition, and γ_e denotes the dissipation rate of the $|e\rangle$ level. (b) The quantum jumps from the $|f\rangle$ level at rate γ_f are only recorded by the environment, and this missing information necessitates a hybrid-Liouvillian formalism (see main text).

Our experiment uses the lowest three energy levels ($|g\rangle$, $|e\rangle$, and $|f\rangle$) of a transmon superconducting circuit [36] that consists of a pair of Josephson junctions in a superconducting quantum interference device (SQUID) geometry shunted by a capacitor. The transmon circuit is placed within a three-dimensional copper microwave cavity that serves two purposes in the experiment. First, it mediates the interaction between the circuit and a nonuniform density of states of the electromagnetic field, allowing us to tune the dissipation rates of the transmon energy levels such that γ_e (the decay rate of the $|e\rangle$ level) is much larger than γ_f (the decay rate of the $|f\rangle$ level). Second, the dispersive interaction between cavity mode and the circuit results in a state-dependent cavity resonance frequency [37]. We achieve a high-fidelity, single-shot readout of the transmon state by probing the cavity with a weak microwave signal and detecting its phase shift.

The dynamics of this three-level quantum system [Fig. 1(b)] is described by a Lindblad master equation

$$\frac{\partial \rho_{\text{tot}}}{\partial t} = -i[H_{\text{c}}, \rho_{\text{tot}}] + \sum_{k=e,f} \left[L_k \rho_{\text{tot}} L_k^\dagger - \frac{1}{2}\{L_k^\dagger L_k, \rho_{\text{tot}}\} \right], \quad (1)$$

where ρ_{tot} denotes a 3×3 density operator. The jump operators $L_e = \sqrt{\gamma_e}|g\rangle\langle e|$ and $L_f = \sqrt{\gamma_f}|e\rangle\langle f|$ describe the energy decay from $|e\rangle$ to $|g\rangle$ and from $|f\rangle$ to $|e\rangle$, respectively. Here we only consider a drive at the $\{|e\rangle, |f\rangle\}$ submanifold, and in the rotating frame $H_{\text{c}} = J(|e\rangle\langle f| + |f\rangle\langle e|) + \Delta/2(|e\rangle\langle e| - |f\rangle\langle f|)$, where Δ is the frequency detuning (relative to the $|e\rangle$—$|f\rangle$ transition) of the microwave drive that couples the states at rate J. The dissipative dynamics of the qutrit to its steady state can be captured by a Liouvillian superoperator defined by Eq. (1), exhibiting the so-called Liouvillian EPs [34,38,39]. A classical analogy of this EP transition is a damped harmonic oscillator, where an EP (corresponding to the critical damping) marks the transition from an overdamped to an underdamped regime [34,38,39].

We utilize the high-fidelity single-shot readout to isolate dynamics in the $\{|e\rangle, |f\rangle\}$ submanifold by eliminating any experimental trials where the qubit undergoes a jump to the state $|g\rangle$ [27]. The resulting dynamics in the submanifold is governed by

$$\frac{\partial \rho}{\partial t} = -i(H_{\text{eff}}\rho - \rho H_{\text{eff}}^\dagger) + L_f \rho L_f^\dagger \quad (2)$$

where ρ denotes a 2×2 density operator. The effective non-Hermitian Hamiltonian $H_{\text{eff}} = H_{\text{c}} - iL_e^\dagger L_e/2 - iL_f^\dagger L_f/2$ takes into account the coherent nonunitary dissipations of both levels and possesses a second-order EP at $J_{\text{EP}} = (\gamma_e - \gamma_f)/4$ and $\Delta = 0$. This EP separates "broken" and "unbroken" regions of effective parity-time (PT) symmetry, where the difference between eigenvalues is either purely imaginary, or purely real. As shown in Eq. (2), if there are no

quantum jumps from the $|f\rangle$ level ($L_f = 0$), or these jumps can be removed from the dynamics using postselection, the system would evolve coherently under H_{eff}.

To capture the effect of jumps from the $|f\rangle$ level, we adopt a hybrid-Liouvillian formalism [35], which describes the non-Hermitian dynamics of an open quantum system under different postselection efficiencies. The dissipative dynamics of the qubit is then written as

$$\frac{\partial \rho}{\partial t} = (\mathcal{L}_0 + \mathcal{L}_1)\rho. \quad (3)$$

Here, the qubit dynamics is captured by two hybrid-Liouvillian superoperators $\mathcal{L}_0\rho \equiv -i(H_{\text{eff}}\rho - \rho H_{\text{eff}}^\dagger)$ and $\mathcal{L}_1\rho \equiv L_f\rho L_f^\dagger$. Compared with the Liouvillian superoperator defined by Eq. (1), the hybrid-Liouvillian superoperator does not lead to a completely positive and trace-preserving map [35]. In contrast to the non-Hermitian Hamiltonian approach based on a Hilbert space of dimension $N = 2$, this hybrid-Liouvillian formalism is based on a Liouville space of dimension $N^2 = 4$. In the Liouville space, ρ is represented as a 4×1 vector, and $\mathcal{L}_{i=0,1}$ is represented as a 4×4 non-Hermitian matrix. Because $\mathcal{L}_0$ encodes the evolution due to H_{eff}, it also exhibits an EP (denoted as "HLEP") at $J = (\gamma_e - \gamma_f)/4$ and $\Delta = 0$. One key difference is that three eigenvectors of $\mathcal{L}_0$ coalesce at the EP, implying that a second-order Hamiltonian EP corresponds to a third-order HLEP [40].

In addition, the non-Hermitian qubit can also suffer from pure dephasing at a rate γ_ϕ, described by a jump operator $L_\phi = \sqrt{\gamma_\phi/2}\sigma_z$. Its effect includes two aspects: on one hand, it modifies H_{eff} (and subsequently $\mathcal{L}_0$) by adding a term $-i\gamma_\phi I/4$ (I denotes an identity operator), which only shifts the overall loss and does not affect the position of EP in the parameter space; on the other hand, it provides another perturbation of quantum jumps, the effect of which can be included in $\mathcal{L}_1$ [41].

Before proceeding to our experiments, we summarize the possible scenarios of non-Hermitian dynamics of an open quantum system. Depending on the postselection efficiency η of quantum jumps through all possible channels, the resulting non-Hermitian dynamics is described by (i) a Liouvillian superoperator with $\eta = 0$, i.e., no postselection; (ii) a hybrid-Liouvillian superoperator with $0 < \eta < 1$, i.e., imperfect postselection; and (iii) an effective non-Hermitian Hamiltonian with $\eta = 1$, i.e., perfect postselection [35]. In the semiclassical limit, the quantum jumps are neglected, that is, equivalent to $\eta = 1$; subsequently, the dynamics of a dissipative classical system can be described by an effective non-Hermitian Hamiltonian [34].

We first investigate the quantum-jump-induced decoherence in the PT-symmetry unbroken regime. Figure 2(a) shows the complex eigenvalues λ of the hybrid-Liouvillian superoperator $(\mathcal{L}_0 + \mathcal{L}_1)$ in the
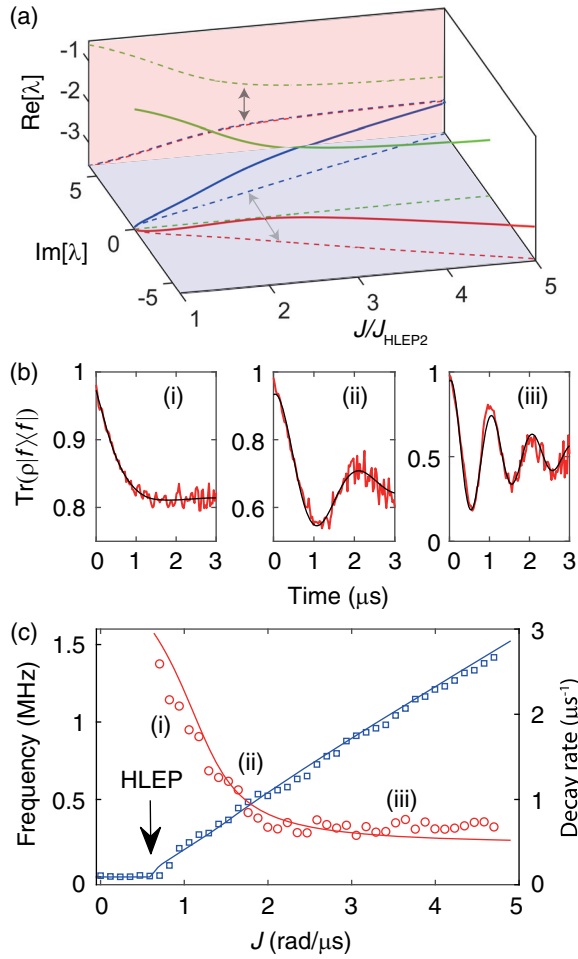
FIG. 2. (a) Complex eigenvalues of the hybrid-Liouvillian superoperator $\mathcal{L}_0 + \mathcal{L}_1$ in the unbroken regime (solid curves). The dashed curves are the projections of the eigenvalues on the J–Re$[\lambda]$ and J–Im$[\lambda]$ planes. The arrows mark the eigenvalue difference. J is normalized by the value at the second-order hybrid-Liouvillian EP (J_{HLEP2}). Only three of the four Liouvillian eigenvalues involved in this study are shown. The blue dashed curve on the J–Re$[\lambda]$ plane has been slightly offset for clarity. (b) Population dynamics versus evolution time for three different values of J, marked by (i)–(iii) in (c). The red curves are experimental results, and the black curves are fits to decaying sine function. (c) The measured oscillation frequency (blue squares, left axis) and decay rate (red circles, right axis) for different drive amplitudes J. The solid lines are calculated from the Liouvillian spectra, where the dissipation rates $\gamma_e = 4.5~\mu\mathrm{s}^{-1}$, $\gamma_f = 0.3~\mu\mathrm{s}^{-1}$, and $\gamma_\phi = 0.5~\mu\mathrm{s}^{-1}$ are used.

unbroken regime, with the real and imaginary parts indicated as projections. Note that the roles of the imaginary and real parts of Hamiltonian and hybrid-Liouvillian spectra are reversed because the "$-i$" term in Eq. (2) is absorbed into the hybrid-Liouvillian superoperator. The perturbative effect of quantum jumps ($\mathcal{L}_1$) lifts the degeneracy of the third-order HLEP of $\mathcal{L}_0$ and generates a new second-order HLEP (see Supplemental Material [41] for further details). By lifting the degeneracy, this perturbation

leads to decoherence, whose rate is determined by the real part of the eigenvalue difference. The effect of the perturbation is enhanced by proximity to the EP due to the cube-root topology of the third-order degeneracy of $\mathcal{L}_0$ [35,41].

To experimentally measure the decoherence rates in the vicinity of the HLEP, we initialize the circuit in the $|f\rangle$ state and then apply a microwave drive with amplitude J. We take 10^4 measurements per time point and only keep the results with the transmon remaining in the $\{|e\rangle, |f\rangle\}$ submanifold for analysis. We record the final $|f\rangle$ population as a function of time. These dynamics are characterized by damped oscillatory behavior of the population, as shown in Fig. 2(b). We extract the decoherence rate and oscillation frequency for different values of J, as shown in Fig. 2(c). The observed damping rates and oscillation frequencies are in good agreement with the real and imaginary parts of hybrid-Liouvillian spectra, respectively. In particular, we note that by proximity to the HLEP, the dissipation is dramatically enhanced over its background rate (i.e., the rate when far from the HLEP).

We now turn to the PT-symmetry broken regime, where the quantum jumps compete with the relative non-Hermitian gain and loss effects. In the absence of quantum jumps, the qubit has two stationary states, corresponding to the two eigenstates $|\pm\rangle$ of H_{eff} [Fig. 3(a)]. The corresponding eigenvalues are purely imaginary. Recalling that imaginary eigenvalues correspond to gain or loss, here with $0 \geq \mathrm{Im}[\lambda_+] > \mathrm{Im}[\lambda_-]$, both states exhibit loss, but the $|+\rangle$ state has gain relative to $|-\rangle$. Therefore, the non-Hermitian dynamics favor the $|+\rangle$ state. The eigenmatrices $\rho_{0,3}$ of $\mathcal{L}_0$ with the smallest and largest damping rates represent the same states, i.e., $\rho_0 \propto |+\rangle\langle+|, \rho_3 \propto |-\rangle\langle-|$. With the perturbation of quantum jumps ($\mathcal{L}_1$), the eigenmatrix ρ_0 becomes slightly mixed $\rho_0 \to \tilde{\rho}_0$ and corresponds to the effective steady state of the non-Hermitian qubit, while the eigenmatrix $\rho_3 \to \tilde{\rho}_3$, a state that is not physically accessible [Fig. 3(a)].

The physical intuition can be understood at the quantum trajectory level. Given a trajectory with only a single quantum jump from the $|f\rangle$ to $|e\rangle$ level, the jump places the qubit in a superposition of $|+\rangle$ and $|-\rangle$. After that, though no further quantum jumps occur, the non-Hermiticity (of H_{eff}) selects the eigenstate with less loss, and the renormalization of the state subsequently leads to a nonexponential decay [31–33]. Hence, the eigenstate $|-\rangle$ of H_{eff} is unstable and will decay to a steady state in a process that involves both quantum jumps and the non-Hermitian (gain versus loss) evolution. Figure 3(a) displays an illustration of one possible trajectory. Since the trajectories contain an unknown number of quantum jumps, the steady state is slightly mixed rather than at the eigenstate $|+\rangle$.

This prediction is experimentally confirmed through quantum state tomography. Here, we prepare the qubit at the eigenstate $|-\rangle$ of H_{eff}, and measure the expectation values of the qubit Pauli operators $\{x, y, z\} \equiv \{\langle\sigma_x\rangle, \langle\sigma_y\rangle, \langle\sigma_z\rangle\}$. Figure 3(b) displays these expectation values for different
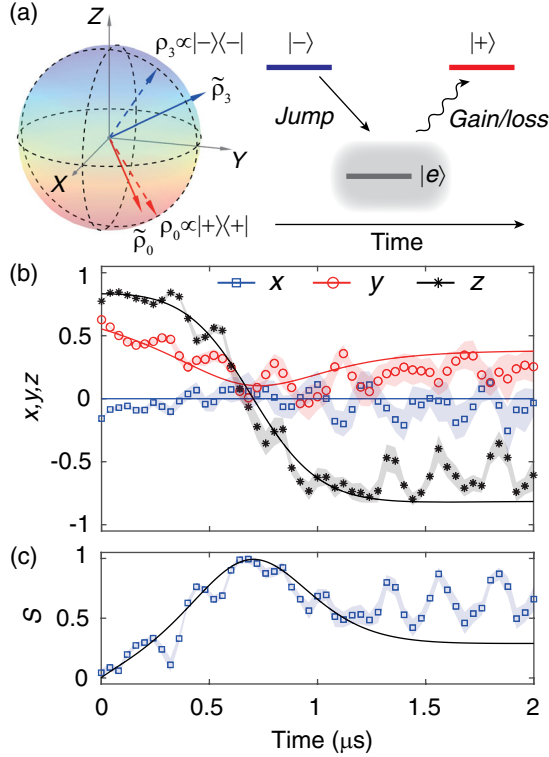
FIG. 3. (a) Left: illustration of the eigenstates and Liouvillian eigenvectors on the Bloch sphere. With no quantum jumps, the two eigenstates $|\pm\rangle$ of $H_{\rm eff}$ represent the same states as two of the Liouvillian eigenvectors ($\rho_{0,3}$, dashed blue and red arrows). With quantum jumps, the two eigenvectors are perturbed: one corresponds to the steady state ($\tilde{\rho}_0$, solid red arrow), and the other one is outside of the Bloch sphere and corresponds to an unphysical state ($\tilde{\rho}_3$, blue solid arrow). Right: illustration of one quantum trajectory with the qubit prepared at $|-\rangle$, where the qubit first jumps to the $|e\rangle$ level and then evolves to $|+\rangle$ due to the non-Hermitian gain and loss effects. (b),(c) Time evolution of the Bloch components (b) and the entropy (c) with the qubit initially prepared at the eigenstate of $H_{\rm eff}$ with more loss. $J = 0.85$ rad μs^{-1} places the system in the PT-symmetry broken regime. The symbols are experimental results, with shaded bands indicating the experimental uncertainty [41], and the curves are theoretical results from Eq. (3). The parameters used are $\gamma_e = 6.38$ μs^{-1}, $\gamma_f = 0.24$ μs^{-1}, and $\gamma_\phi = 0.9$ μs^{-1}. Residual oscillations in the data are likely due to technical fluctuations of the tomography calibration.

evolution times. We highlight several features of the evolution that are different than the dissipative evolution of a Hermitian qubit, where we expect exponential decay to steady state. The non-Hermitian evolution, perturbed by quantum jumps, exhibits (i) nonexponential evolution, (ii) occurring on a timescale much faster than the quantum jump rate γ_f. This occurs due to the nonzero overlap $\langle -|f\rangle$; jumps from $|f\rangle$ to $|e\rangle$ create a mixed state. Thereafter the relative gain of the $|+\rangle$ state causes its population to grow, leading to the nonexponential population evolution. This is further confirmed by examining the evolution of the entropy, defined as

$S \equiv -\sum p_i \log_2(p_i)$, where p_i is the eigenvalue of the density matrix ρ of the qubit [Fig. 3(c)]. The quantum jumps increase the entropy; this distinguishes the evolution from imperfect (pure) eigenstate preparation, which would also seed non-Hermitian evolution toward $|+\rangle$, but with fixed zero entropy [42].

Finally, we study the qubit dynamics under slow parameter variation to reveal the effects of quantum jumps on non-Hermitian adiabatic evolution. We choose a straight parameter path with $J = 30$ rad μs^{-1} ($\gg J_{\rm EP} = 1.5$ rad μs^{-1}) and $\Delta = -30\pi \sin(2\pi t/T)$ rad μs^{-1}, where $T = 4$ μs is the loop period [Fig. 4(a)]. The initial state at $t = 0$ is chosen to be an eigenstate of $H_{\rm eff}$ (approximated as $|+x\rangle$). Along this parameter path, the energy gap is large enough to satisfy the slow-driving condition $T|\lambda_+ - \lambda_-| \gg 1$. For $t < T/2$, the initial state follows the instantaneous eigenstate $|+\rangle$ with relative gain. At $t = T/2$, the parameter path crosses a branch cut for the imaginary Riemann surface at $\Delta = 0$. Here, the instantaneous eigenstates exhibit a loss-switch behavior; the eigenstate with relative gain becomes the eigenstate with more loss [Fig. 4(b)].

The results of quantum state tomography are shown in Fig. 4(c). At $t = 2$ μs, adiabatic evolution would return the qubit to the state $|+x\rangle$. The qubit returns close to this state, with slight mixing induced by the quantum jumps. For $t > T/2$ the qubit is now predominantly in the eigenstate with greater loss, seeding non-Hermitian evolution toward the eigenstate $|-\rangle$. At the end of the parameter sweep, the qubit has undergone a switch between eigenstates, induced by the small perturbation of quantum jumps. This transition is accompanied by a sharp increase in the entropy as shown in Fig. 4(d).

Similar nonadiabatic state or energy transfer has been observed when dynamically encircling an EP [21–24] as a result of nonadiabatic coupling between eigenstates and non-Hermitian gain and loss effects [43]. To verify that our parameter variation is sufficiently slow to prevent this nonadiabatic coupling, we plot the calculated dynamics in the absence of quantum jumps in Fig. 4(c), observing that there is no eigenstate switch. This reveals how quantum jumps effectively serve as a new source of nonadiabatic coupling, breaking adiabatic evolution even when parameter variation is sufficiently slow.

Quantum jumps, even when introduced at very modest rates, produce significant effects on non-Hermitian dynamics. The dissipation induced by these jumps is greatly enhanced by proximity to the EP, with dynamics driven by non-Hermitian evolution. In addition, quantum jumps introduce a new timescale relevant to adiabatic state transport in non-Hermitian systems. Our study elucidates the role and effect of dissipation on quantum non-Hermitian evolution, highlighting how controlling these dissipation mechanisms will be critical for harnessing non-Hermiticity and complex energies in quantum information processing and quantum sensing [40,44–48].
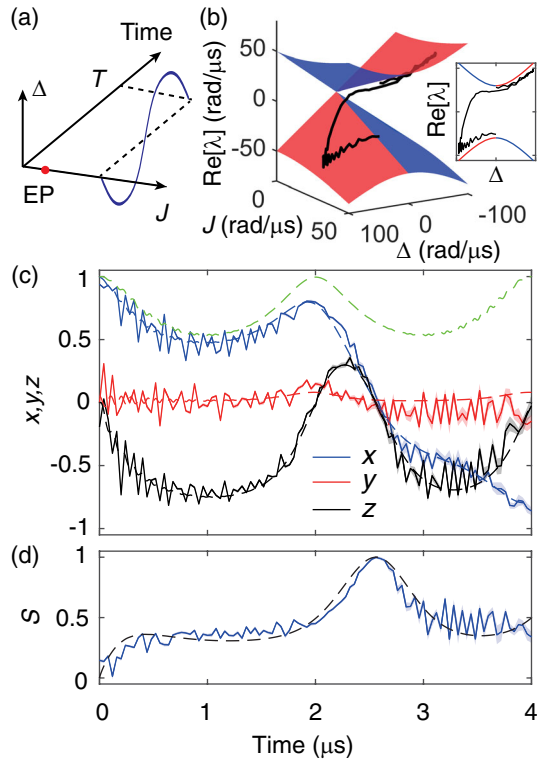
FIG. 4. (a) Illustration of the parameter path in the parameter space. (b) The real part of the Riemann surface, where the red (blue) surface represents the energy surface with relative gain (loss). The real part of the energy of the qubit ($\mathrm{Tr}[\rho H_{\mathrm{eff}}]$) along the trajectory is plotted on the Riemann surface (black line) and also shown in the inset. The time evolution of the Bloch components (c) and the entropy of the corresponding density matrix (d) are displayed for the initial state $|+x\rangle$ and the loop period $T = 4 \mu$s. The solid curves are experimental results, with shaded bands indicating the experimental uncertainty [41], and the dashed curves are calculations from Eq. (3). For comparison, the evolution of the x component with no quantum jumps (due to $\mathcal{L}_0$ only) is also shown [dashed green curve in (c)]. The parameters used are $\gamma_e = 6.34 \ \mu\mathrm{s}^{-1}$, $\gamma_f = 0.26 \ \mu\mathrm{s}^{-1}$, and $\gamma_\phi = 0.5 \ \mu\mathrm{s}^{-1}$.

*wchen34@wustl.edu
†murch@physics.wustl.edu

[1] M. A. Miri and A. Alù, Exceptional points in optics and photonics, Science **363**, eaar7709 (2019).

[2] S. K. Özdemir, S. Rotter, F. Nori, and L. Yang, Parity–time symmetry and exceptional points in photonics, Nat. Mater. **18**, 783 (2019).

[3] C. Dembowski, H.-D. Gräf, H. L. Harney, A. Heine, W. D. Heiss, H. Rehfeld, and A. Richter, Experimental Observation of the Topological Structure of Exceptional Points, Phys. Rev. Lett. **86**, 787 (2001).

[4] C. E. Rüter, K. G. Makris, R. El-Ganainy, D. N. Christo-doulides, M. Segev, and D. Kip, Observation of parity-time symmetry in optics, Nat. Phys. **6**, 192 (2010).

[5] B. Peng, Ş. K. Özdemir, F. Lei, F. Monifi, M. Gianfreda, G. L. Long, S. Fan, F. Nori, C. M. Bender, and L. Yang, Parity-time-symmetric whispering-gallery microcavities, Nat. Phys. **10**, 394 (2014).

[6] J. Schindler, Z. Lin, J. M. Lee, H. Ramezani, F. M. Ellis, and T. Kottos, PT-symmetric electronics, J. Phys. A **45**, 444029 (2012).

[7] C. M. Bender, B. K. Berntson, D. Parker, and E. Samuel, Observation of PT phase transition in a simple mechanical system, Am. J. Phys. **81**, 173 (2013).

[8] C. Shi, M. Dubois, Y. Chen, L. Cheng, H. Ramezani, Y. Wang, and X. Zhang, Accessing the exceptional points of parity-time symmetric acoustics, Nat. Commun. **7**, 11110 (2016).

[9] X. Zhu, H. Ramezani, C. Shi, J. Zhu, and X. Zhang, PT-Symmetric Acoustics, Phys. Rev. X **4**, 031042 (2014).

[10] J. Li, A. K. Harter, J. Liu, L. de Melo, Y. N. Joglekar, and L. Luo, Observation of parity-time symmetry breaking transitions in a dissipative Floquet systems of ultracold atoms, Nat. Commun. **10**, 855 (2019).

[11] M. Partanen *et al.*, Exceptional points in tunable super-conducting resonators, Phys. Rev. B **100**, 134505 (2019).

[12] B. Peng, Ş. K. Özdemir, M. Liertzer, W. Chen, J. Kramer, H. Yılmaz, J. Wiersig, S. Rotter, and L. Yang, Chiral modes and directional lasing at exceptional points, Proc. Natl. Acad. Sci. U.S.A. **113**, 6845 (2016).

[13] M. Brandstetter, M. Liertzer, C. Deutsch, P. Klang, J. Schöberl, H. E. Türeci, G. Strasser, K. Unterrainer, and S. Rotter, Reversing the pump dependence of a laser at an exceptional point, Nat. Commun. **5**, 4034 (2014).

[14] Z. J. Wong, Y.-L. Xu, J. Kim, K. O'Brien, Y. Wang, L. Feng, and X. Zhang, Lasing and anti-lasing in a single cavity, Nat. Photonics **10**, 796 (2016).

[15] J. Wiersig, Enhancing the Sensitivity of Frequency and Energy Splitting Detection by Using Exceptional Points: Application to Microcavity Sensors for Single-Particle Detection, Phys. Rev. Lett. **112**, 203901 (2014).

[16] W. Chen, S. K. Özdemir, G. Zhao, J. Wiersig, and L. Yang, Exceptional points enhance sensing in an optical micro-cavity, Nature (London) **548**, 192 (2017).

[17] H. Hodaei, A. U. Hassan, S. Wittek, H. Garcia-Gracia, R. El-Ganainy, D. N. Christodoulides, and M. Khajavikhan, Enhanced sensitivity at higher-order exceptional points, Nature (London) **548**, 187 (2017).

[18] W. Langbein, No exceptional precision of exceptional-point sensors, Phys. Rev. A **98**, 023805 (2018).

[19] H.-K. Lau and A. A. Clerk, Fundamental limits and non-reciprocal approaches in non-Hermitian quantum sensing, Nat. Commun. **9**, 4320 (2018).

[20] M. Zhang, W. Sweeney, C. W. Hsu, L. Yang, A. D. Stone, and L. Jiang, Quantum Noise Theory of Exceptional Point Amplifying Sensors, Phys. Rev. Lett. **123**, 180501 (2019).

[21] H. Xu, D. Mason, L. Jiang, and J. G. Harris, Topological energy transfer in an optomechanical system with excep-tional points, Nature (London) **537**, 80 (2016).

[22] J. Doppler, A. A. Mailybaev, J. Böhm, U. Kuhl, A. Girschik, F. Libisch, T. J. Milburn, P. Rabl, N. Moiseyev, and S. Rotter, Dynamically encircling an exceptional point for asymmetric mode switching, Nature (London) **537,** 76 (2016).

[23] Y. Choi, C. Hahn, J. W. Yoon, S. H. Song, and P. Berini, Extremely broadband, on-chip optical nonreciprocity enabled by mimicking nonlinear anti-adiabatic quantum jumps near exceptional points, Nat. Commun. **8,** 14154 (2017).

[24] X. L. Zhang, S. Wang, B. Hou, and C. T. Chan, Dynamically Encircling Exceptional Points: In Situ Control of Encircling Loops and the Role of the Starting Point, Phys. Rev. X **8,** 021066 (2018).

[25] Y. Wu, W. Liu, J. Geng, X. Song, X. Ye, C.-K. Duan, X. Rong, and J. Du, Observation of parity-time symmetry breaking in a single-spin system, Science **364,** 878 (2019).

[26] W. Liu, Y. Wu, C.-K. Duan, X. Rong, and J. Du, Dynamically Encircling an Exceptional Point in a Real Quantum System, Phys. Rev. Lett. **126,** 170506 (2021).

[27] M. Naghiloo, M. Abbasi, Y. N. Joglekar, and K. W. Murch, Quantum state tomography across the exceptional point in a single dissipative qubit, Nat. Phys. **15,** 1232 (2019).

[28] L. Xiao *et al.*, Observation of topological edge states in parity time symmetric quantum walks, Nat. Phys. **13,** 1117 (2017).

[29] F. Klauck, L. Teuber, M. Ornigotti, M. Heinrich, S. Scheel, and A. Szameit, Observation of PT-symmetric quantum interference, Nat. Photonics **13,** 883 (2019).

[30] S. Yu *et al.*, Experimental Investigation of Quantum $\mathcal{PT}$-Enhanced Sensor, Phys. Rev. Lett. **125,** 240506 (2020).

[31] J. Dalibard, Y. Castin, and K. Mølmer, Wave-Function Approach to Dissipative Processes in Quantum Optics, Phys. Rev. Lett. **68,** 580 (1992).

[32] K. Mølmer, Y. Castin, and J. Dalibard, Monte Carlo wave-function method in quantum optics, J. Opt. Soc. Am. B **10,** 524 (1993).

[33] M. B. Plenio and P. L. Knight, The quantum-jump approach to dissipative dynamics in quantum optics, Rev. Mod. Phys. **70,** 101 (1998).

[34] F. Minganti, A. Miranowicz, R. W. Chhajlany, and F. Nori, Quantum exceptional points of non-Hermitian Hamiltonians and Liouvillians: The effects of quantum jumps, Phys. Rev. A **100,** 062131 (2019).

[35] F. Minganti, A. Miranowicz, R. W. Chhajlany, I. I. Arkhipov, and F. Nori, Hybrid-Liouvillian formalism connecting exceptional points of non-Hermitian Hamiltonians and Liouvillians via postselection of quantum trajectories, Phys. Rev. A **101,** 062112 (2020).

[36] J. Koch, T. M. Yu, J. Gambetta, A. A. Houck, D. I. Schuster, J. Majer, A. Blais, M. H. Devoret, S. M. Girvin, and R. J. Schoelkopf, Charge-insensitive qubit design derived from the Cooper pair box, Phys. Rev. A **76,** 042319 (2007).

[37] A. Wallraff, D. I. Schuster, A. Blais, L. Frunzio, J. Majer, M. H. Devoret, S. M. Girvin, and R. J. Schoelkopf, Approaching Unit Visibility for Control of a Superconducting Qubit with Dispersive Readout, Phys. Rev. Lett. **95,** 060501 (2005).

[38] N. Hatano, Exceptional points of the Lindblad operator of a two-level system, Mol. Phys. **117,** 2121 (2019).

[39] I. I. Arkhipov, A. Miranowicz, F. Minganti, and F. Nori, Quantum and semiclassical exceptional points of a linear system of coupled cavities with losses and gain within the Scully-Lamb laser theory, Phys. Rev. A **101,** 013812 (2020).

[40] J. Wiersig, Robustness of exceptional-point-based sensors against parametric noise: The role of Hamiltonian and Liouvillian degeneracies, Phys. Rev. A **101,** 053846 (2020).

[41] See Supplemental Material at http://link.aps.org/supplemental/10.1103/PhysRevLett.127.140504 which provides extensive detail on the experimental procedures and statistical analysis as well as further information about the calculation of the Liouvillian spectrum.

[42] D. C. Brody and E. M. Graefe, Mixed-State Evolution in the Presence of Gain and Loss, Phys. Rev. Lett. **109,** 230405 (2012).

[43] T. J. Milburn, J. Doppler, C. A. Holmes, S. Portolan, S. Rotter, and P. Rabl, General description of quasiadiabatic dynamical phenomena near exceptional points, Phys. Rev. A **92,** 052124 (2015).

[44] A. Pick, S. Silberstein, N. Moiseyev, and N. Bar-Gill, Robust mode conversion in NV centers using exceptional points, Phys. Rev. Research **1,** 013015 (2019).

[45] P. Kumar, H.-G. Zirnstein, K. Snizhko, Y. Gefen, and B. Rosenow, Optimized quantum steering and exceptional points, arXiv:2101.07284.

[46] P. Kumar, K. Snizhko, and Y. Gefen, Near-unit efficiency of chiral state conversion via hybrid-Liouvillian dynamics, arXiv:2105.02251.

[47] S. Khandelwal, N. Brunner, and G. Haack, Signatures of exceptional points in a quantum thermal machine, arXiv:2101.11553.

[48] F. Minganti, V. Macrì, A. Settineri, S. Savasta, and F. Nori, Dissipative state transfer and Maxwell's demon in single quantum trajectories: Excitation transfer between two non-interacting qubits via unbalanced dissipation rates, Phys. Rev. A **103,** 052201 (2021).